Flow Boiling in Rectangular Microchannels: 1-D Modelling of the Influence of Inlet Resistance on Flow Reversal

Sateesh GEDUPUDI[1,*], David B.R. KENNING[2], Tassos G. KARAYIANNIS[2]

* Corresponding author: Tel.: ++91 (0)44 2257 4721; Email: sateeshg@iitm.ac.in
1 Department of Mechanical Engineering, Indian Institute of Technology Madras, Chennai, India
2 School of Engineering and Design, Brunel University, UK

Abstract Pressure changes caused by the growth of confined bubbles during flow boiling in mini/micro-channels lead to transient flow reversal in the presence of inlet (upstream) compressibility. A 1-D model is presented to study the effect of inlet resistance on maximum flow reversal distance, return time and local pressure fluctuations for different initial upstream compressible volumes for water boiling at atmospheric pressure. The two upstream compressibility models considered are condensable vapour in a subcooled boiling region and trapped non-condensable gas.

Keywords: Confined Bubble, Flow Boiling, Micro-channel, Flow Instability

1. Introduction

Parallel micro-channel heat sinks making use of flow boiling are a potential method of cooling devices that dissipate high heat fluxes, such as microprocessors. Inherent with the confined bubble growth in mini/micro-channels are flow instabilities, which lead to uneven flow distribution between channels, temporary flow reversal and poor heat transfer due to intermittent dry-out.

Zhang et al. (2004 and 2005) and Brutin and Tadrist (2004) measured pressure fluctuations, dependent on the upstream compressibility resulting from different sources. Empirical techniques employed to control flow instabilities include usage of flow resistance at the inlet to individual channels, Kandlikar et al. (2006), Kosar et al. (2006), and enhancement of bubble formation inside the channels, Agostini et al. (2008). Gedupudi et al. (2011) made an experimental observation of bubble growth in a single microchannel with and without inlet compressibility and presented a 1-D model to study the influence of inlet (upstream) compressibility conditions on local pressure fluctuations and flow reversal for various combinations of parameters, for water at 101 kPa in channels without inlet resistance. It was demonstrated by a single example that inlet resistance could greatly reduce flow reversal and transmission of pressure changes to the inlet plenum, but there was little effect on the large amplitude of the pressure fluctuation within the channel. The predicted amplitude of the pressure fluctuations without inlet compressibility was greatly reduced for R134a at 800 kPa. Therefore, use of a coolant boiling at relatively high reduced pressure p/p_c may be a third method for the suppression of flow reversal but raises other issues of mechanical strength and safety. The two upstream compressibility models considered were condensable vapour in a subcooled boiling region in an upstream preheater and non-condensable ideal gas subject to compression with polytropic exponent n. Compressibility due to subcooled boiling may occur in experimental rigs with electrical preheaters or in industrial applications in which heat can be supplied from a high temperature source through a heat exchanger. Compressibility due to accidental trapping of small volumes of non-condensable gas during filling or maintenance is highly likely in most applications. Wang et al. (2011) experimentally investigated bubble confinement and pressure drop fluctuation in a

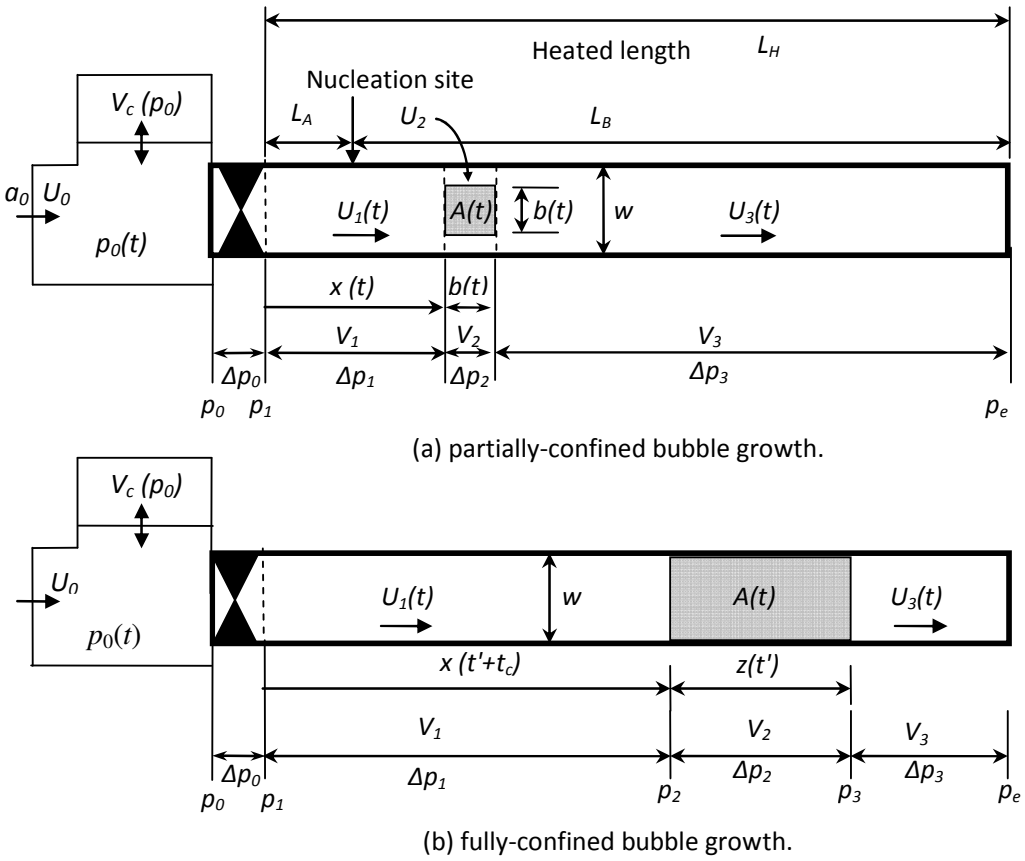

Fig. 1. Bubble growth models

high aspect ratio microchannel. Liu et al. (2013) discussed the diversity of behaviour reported in the literature for microchannel boiling controlling mechanisms and concluded that proper characterization of conditions should include control and specification of the upstream compressibility.

The previous work by Gedupudi et al. (2011) includes just a single case of one inlet resistance value and one initial volume of condensable vapour. The present work makes a detailed study of the effect of inlet resistance on maximum flow reversal distance, return time and local pressure fluctuation for different initial upstream compressible volumes, for water boiling at atmospheric pressure.

2. 1-D Modelling

2.1 Bubble growth

A single channel with high aspect ratio is considered (w>>h). Bubble growth is assumed to occur in two stages: partial confinement (PC) by the minor dimension h, followed by full confinement (FC) by the major dimension w for $t \geq t_c$. Neglecting heat flow through the thicker liquid film on the minor sides and with the approximation that ρ_v is constant,

$$A = A_i e^{t/\tau}, \quad \tau = \rho_v h_{lv} h/q \tag{1}$$

It is assumed during PC that $A = b^2$ (t), increasing exponentially from h^2 at $t = 0$ to w^2 at $t_c = 2\tau$ ln (w/h). During FC, $A = wz = w^2 e^{(t-t_c)/\tau}$. The growth Equation (1) described the observed exponential growth during PC of bubbles forming repeatedly at a single nucleation site on a thick copper wall, Gedupudi et al. (2011). All fluid properties are assumed to be constant, evaluated at the constant channel outlet pressure p_e. A single nucleation site is located at L_A from the inlet, see fig. 1.

2.2 Fluid flow

A constant volumetric flow rate U_0a_0 is delivered by the pump to the upstream plenum of cross-sectional area $a_0 >> wh$ so that $p_0(t)$ is the stagnation pressure. When upstream compressibility is absent, $U_1 = U_0a_0/(wh)$.

2.3 Upstream compressibility

The two upstream (inlet) compressibility models considered, as in Gedupudi et al. (2011), are:

1. Condensable vapour in a subcooled boiling region in an upstream preheater, for which

$$\frac{dV_c}{dt} = -G_c V_c^{2/3}(p_0 - p_{0i}) \quad (2)$$

where $G_c = \frac{4.8\alpha_e T_{sati}}{(\rho_v h_{lv})^2}$ and α_e is the heat transfer coefficient to be determined empirically.

2. Non-condensable ideal gas subject to compression with polytropic exponent *n*, for which

$$\frac{dV_c}{dt} = -\frac{V_{ci} p_{0i}^{1/n}}{p_0^{1+1/n}}\frac{dp_0}{dt}, \approx -C_c\frac{dp_0}{dt}$$ for small isothermal changes. (3)

From the continuity equation,

$$\frac{dV_c}{dt} = whU_1 - a_0U_0 \quad (4)$$

2.4 Viscous pressure drop (Δp_f)

An expression for the Fanning friction factor f_F as a function of Reynolds number Re and the channel aspect ratio α in steady laminar flow from Papautsky et al. (1999), White (1994) and Hartnett and Kostic (1989), (after conversion from Darcy friction factor $f_D = 4f_F$), is combined with a minimum Fanning friction factor $f_F = 0.01$ for turbulent flow. On a Moody chart, this corresponds to transition at about Re = 1500 and a relative roughness of ~ 0.01. This is approximate.

$$f_F Re = 24(1 - 1.3553\alpha + 1.9467\alpha^2 - 1.7012\alpha^3 + 0.9564\alpha^4 - 0.2537\alpha^5)$$

where $0 < \alpha < 1$. (5)

The viscous pressure drop considered here occurs only in the liquid slugs upstream and downstream of the bubble, of lengths L_u and L_d. The total viscous pressure drop is given by

$$\Delta p_f = \Delta p_{f,u} + \Delta p_{f,d} \quad (6)$$

where

$$\Delta p_{f,u} = S_1 \frac{2\rho_l f_{F,u} L_u U_1^2}{D_h} \quad (7)$$

$$\Delta p_{f,d} = S_3 \frac{2\rho_l f_{F,d} L_d U_3^2}{D_h} \quad (8)$$

where $S_1 = |U_1|/U_1$, $S_3 = |U_3|/U_3$.

The stagnation pressure p_0 in the inlet plenum is given by

$$p_0 = p_1 + (1.5K + FS_1)\frac{\rho_l U_1^2}{2}$$

including a minor loss at a sharp-edged channel entry, equal to $0.5\left(\frac{\rho_l U_1^2}{2}\right)$.

K=1 for positive U_1 and equal to 0 for negative U_1 (possible with upstream compressibility). A constant loss coefficient F based on the velocity U_1 is used to model frictional resistance imposed by the restriction at the channel inlet. In the present model, it is assumed that only liquid enters or leaves the upstream end of the channel.

2.5 Pressure changes

From the principle of conservation of momentum, for PC growth, pressure differences, as shown in Fig. 1, are given by

$$\Delta p_1 = \rho_l\left(x\frac{dU_1}{dt}\right) + \Delta p_{f,u} \quad (9)$$

$$\Delta p_2 = \left\{\begin{array}{l}\left[\left(\rho_l\frac{db}{dt}\right) - (\rho_l - \rho_v)\frac{2b}{w}\frac{db}{dt}\right]\frac{(U_1 + U_3)}{2} \\ + \left[(\rho_l b) - (\rho_l - \rho_v)\frac{b^2}{w}\right]\frac{1}{2}\left(\frac{dU_1}{dt} + \frac{dU_3}{dt}\right)\end{array}\right\} \quad (21)$$

$$\Delta p_3 = \rho_l\left[U_3\left(-U_1 - \frac{db}{dt}\right) + (L_H - x - b)\frac{dU_3}{dt}\right] + \left[\rho_l U_3^2 - 0\right] + \Delta p_{f,d} \quad (10)$$

From the above equations, with r as the ratio of vapour density to liquid density, ρ_v / ρ_l,

$$\frac{dU_1}{dt} = \frac{\left(\begin{array}{l} \dfrac{p_1 - p_e}{\rho_1} - \dfrac{\Delta p_f}{\rho_1} - U_1\left[r\dfrac{h^2}{w\tau} e^{t/\tau} \right] \\ - e^{t/\tau} \dfrac{h^2}{w\tau^2}(L_H - x) + e^{3t/2\tau} \dfrac{3h^3}{4w\tau^2} \\ - e^{2t/\tau} \dfrac{h^4}{w^2\tau^2} r \end{array} \right)}{\left[L_H - (1-r)\dfrac{h^2}{w} e^{t/\tau} \right]} \tag{11}$$

For FC growth, pressure differences, as shown in Fig. 1, are given by

$$\Delta p_1 = \rho_l \left(x \frac{dU_1}{dt} \right) + \Delta p_{f,u} \tag{12}$$

$$\Delta p_2 = \left\{ \begin{array}{l} \left[\left(\rho_v \dfrac{dz}{dt} \right) \dfrac{(U_1 + U_3)}{2} \right] \\ + \left[(\rho_v z) \dfrac{1}{2} \left(\dfrac{dU_1}{dt} + \dfrac{dU_3}{dt} \right) \right] \end{array} \right\} \tag{13}$$

$$\Delta p_3 = \rho_l \left[(L_H - x - z) \frac{dU_3}{dt} \right] + \Delta p_{f,d} \tag{14}$$

$$\frac{dU_1}{dt'} = \frac{\left(\begin{array}{l} \dfrac{p_1 - p_e}{\rho_1} - \dfrac{\Delta p_f}{\rho_1} - U_1 \dfrac{rw}{\tau} e^{t'/\tau} \\ - (L_H - x) \dfrac{w}{\tau^2} e^{t'/\tau} + (1-r) \dfrac{w^2}{\tau^2} e^{2t'/\tau} \end{array} \right)}{\left[L_H - (1-r) w e^{t'/\tau} \right]} \tag{15}$$

For vapour venting stage (bubble passage through the channel outlet),

$$\frac{dU_1}{dt} = \frac{(p_1 - p_e) - (\Delta p_f) - \rho_v \left(\dfrac{z^2}{\tau^2} + U_1 \dfrac{z}{\tau} \right)}{\rho_l x + \rho_v z} \tag{16}$$

The equations are solved by a finite difference method. The incoming flow a_0U_0 and the exit pressure p_e are assumed to be constant. The initial velocity is $U_1 = a_0U_0 / wh$. A time step of 10^{-6} s was used. Results obtained with the time steps 10^{-6} and 10^{-5}s deviated by around ± 0.25%.

3. Results and Discussion

Simulations are carried out for a channel dimension 0.3 mm x 1.5 mm x 40 mm with nucleation site at 20 mm from the channel inlet. Results presented are for water at 1.01 bar. Three initial compressible volumes (V_{ci}) at inlet are considered, viz.: 10^{-7} m^3 (5.5 times the channel volume), 5 x 10^{-8} m^3 (2.8 times the channel volume) and 1 x 10^{-8} m^3 (about half the channel volume). The values of heat flux q and initial channel inlet velocity U_{1i} are 200 kW/m^2 and 0.4 m/s respectively. For the condensable vapour compressibility model, the constant G_c (eqn.2) is 4 x 10^{-5} m^3/N-s (based on the assumed evaporative heat transfer coefficient).

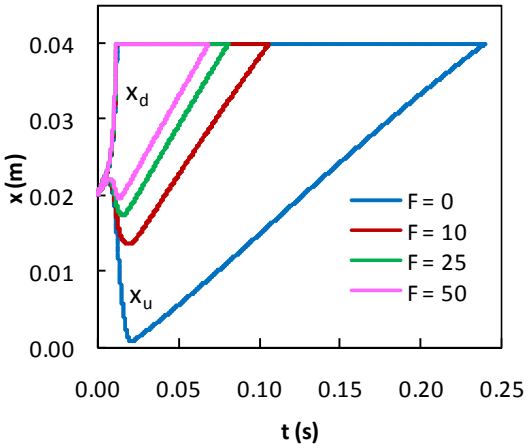

Fig. 2. Bubble upstream and downstream locations (x_u and x_d) for different F values. V_{ci} = 1.0 x 10^{-7} m^3 (condensable vapour due to subcooled boiling).

Fig. 2 shows the position (upstream and downstream ends) of the bubble originating at the channel midpoint, for different inlet restriction factors, F. With increasing F, the maximum flow reversal distance (distance the bubble travels upstream) decreases. The decrease is almost 75% as F increases from zero to 10. Further reductions with the increase in F are smaller. For the conditions specified, there is very little effect of F on the motion of the downstream end of the bubble.

Fig. 3 shows the transient pressure changes across the downstream liquid slug (p_3 – p_e)

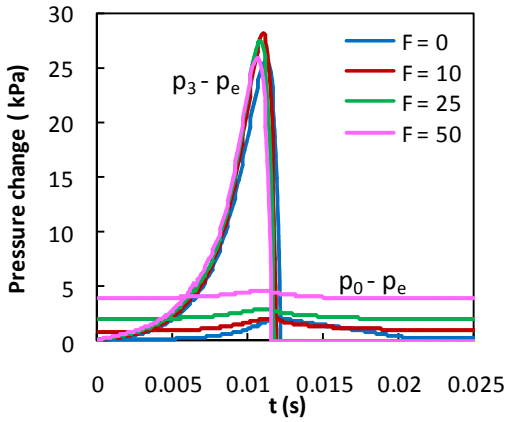

Fig. 3. Transient pressure changes for different F values. V_{ci} = 1.0 x 10^{-7} m^3, condensable vapour.

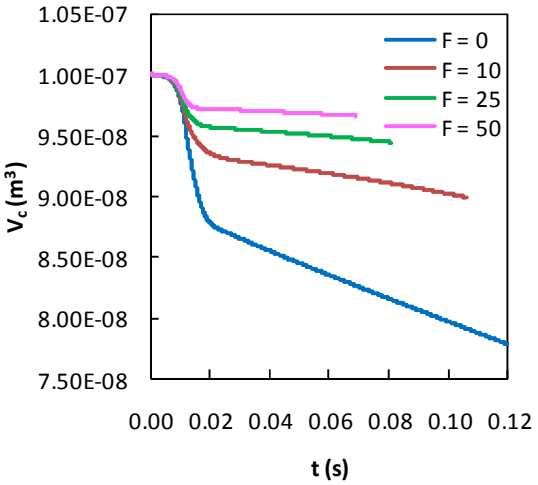

Fig. 4. Evolution of inlet compressible volume (condensable vapour due to subcooled boiling) for different F values. V_{ci} = 1.0 x 10^{-7} m^3.

and the channel ($p_0 - p_e$). With increasing F from zero to 10, peak $p_3 - p_e$ increases by little due to the increased acceleration downstream, and with further increase in F, peak $p_3 - p_e$ decreases due to the decrease in the length of the downstream liquid slug. The magnitude of $p_0 - p_e$ increases and the fluctuation in $p_0 - p_e$ decreases with the increase in F and it almost remains constant at higher F. It may be noted that the local pressure fluctuation ($p_3 - p_e$) remains higher though flow reversal is minimized at higher F. Fig. 4 shows the evolution of inlet compressible volume (condensable vapour). A sharp change in V_c corresponds to the change in $p_0 - p_e$ (Fig.3) as evident from equation (2).

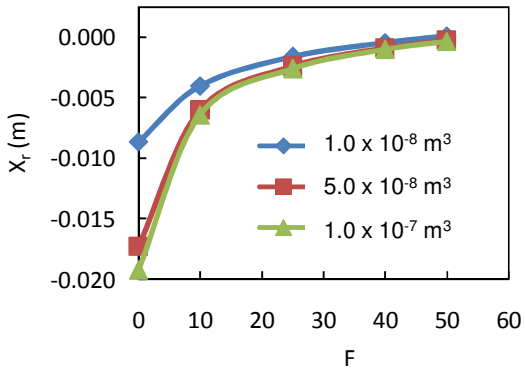

Fig. 5. Effect of inlet resistance on maximum flow reversal distance (negative) for three different V_{ci} values due to subcooled boiling.

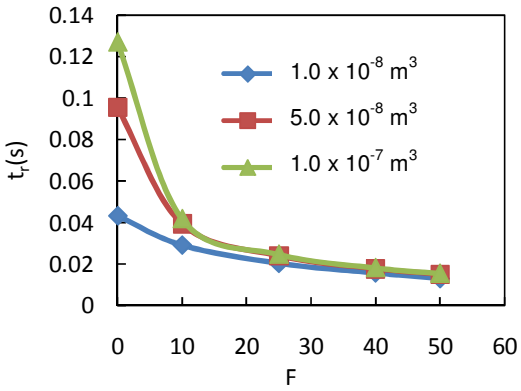

Fig. 6. Effect of inlet resistance on bubble (upstream end) return time for three different V_{ci} values due to subcooled boiling.

Fig. 5 shows a typical effect of the inlet restriction on flow reversal. With the largest compressible volume and no inlet resistance, there is a strong flow reversal that nearly reaches the inlet plenum. This is much reduced by increasing F, with only small further improvement for F >20, which is nearly the case even with the smallest compressible volume. The time taken (from the beginning) for the upstream end of the bubble to reach the initial point after the flow reversal (second reversal, strictly speaking) decreases almost asymptotically, Fig. 6. Figures 7-13 show the effect of inlet compressibility due to non-condensable gas, all other conditions being the same as those for sub-cooled boiling (condensable vapour) case.

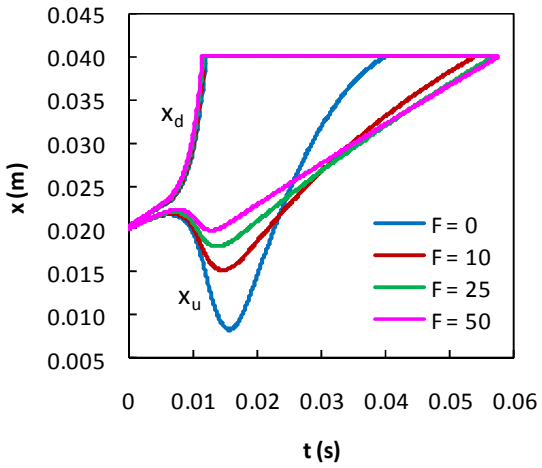

Fig. 7. Bubble upstream and downstream locations (x_u and x_d) for different F values.V_{ci} = 1.0 x 10^{-7} m^3 (non-condensable gas).

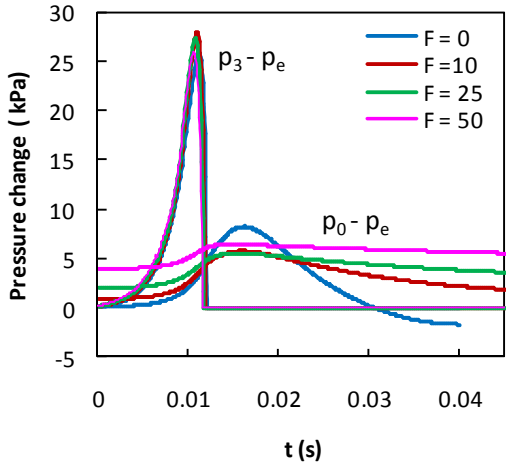

Fig. 8. Transient pressure changes for different F values. V_{ci} = 1.0 x 10^{-7} m^3, non-condensable gas.

Flow reversal decreases with the increase in F, Fig. 7. Peak pressures ($p_0 - p_e$, $p_3 - p_e$) are nearly the same as those for the condensable vapour case, except that the fluctuation in $p_0 - p_e$ is little higher, Fig. 8. The evolution of compressible volume in Fig. 9 closely follows the change in $p_0 - p_e$ in Fig. 8, as evident from eqn (3). Figures 10 and 11 show the motion of the bubble upstream and downstream ends for V_{ci} = 5.0 x 10^{-8} m^3 and 1.0 x 10^{-8} m^3 respectively. For F = 0 case, the bubble at the

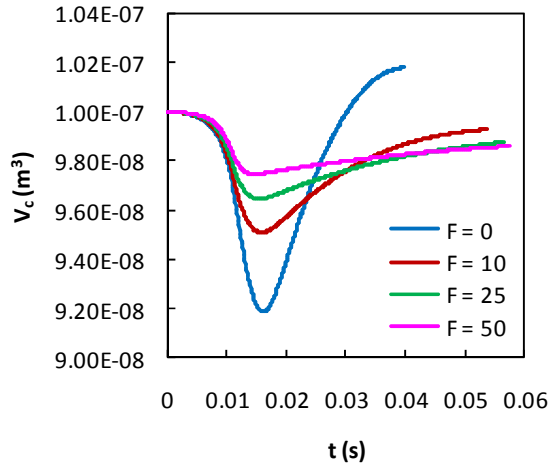

Fig. 9. Evolution of inlet compressible volume (non-condensable gas) for different F values. V_{ci} = 1.0 x 10^{-7} m^3.

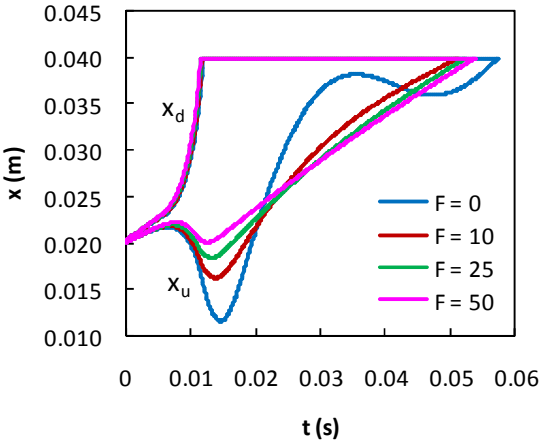

Fig. 10. Bubble upstream and downstream locations (x_u and x_d) for different F values. V_{ci} = 5.0 x 10^{-8} m^3 (non-condensable gas).

upstream end oscillates and the frequency of oscillation is higher for smaller V_{ci} (Fig. 11). This is inline with the physics that the system with inlet compressibility due to non-condensable gas acts like a spring-mass system using the upstream mass of the liquid column in the channel, as discussed in Gedupudi et al. (2011). These oscillations and flow reversal get suppressed with increasing F, as shown in these two Figures. The maximum flow reversal distance decreases with increasing *F* and this change diminishes as F increases. For smaller V_{ci}, this distance will be zero at lower *F* itself, Fig. 12. The variation of bubble

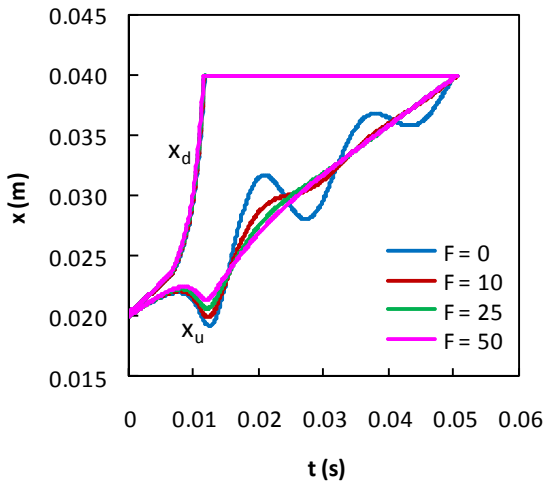

Fig.11. Bubble upstream and downstream locations (x_u and x_d) for different F values. V_{ci} = 1.0 x 10^{-8} m^3 (non-condensable gas).

(upstream end) return time with *F*, as shown in Fig. 13, is not quite the same as that for condensable vapour case (Fig.6). This is because the return time is influenced by the flow oscillation, as can be seen in Figs. 7, 10 and 11.

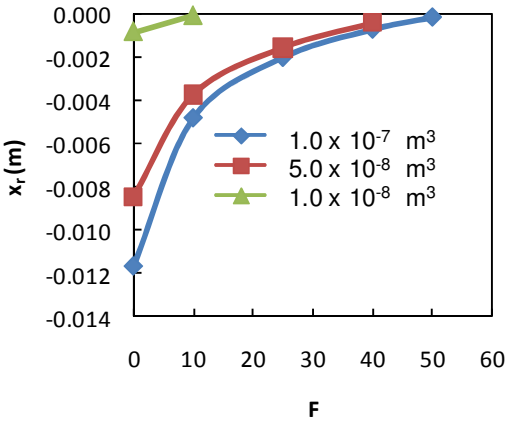

Fig. 12. Effect of inlet resistance on maximum flow reversal distance (negative) for three different V_{ci} due to non-condensable gas.

4. Conclusions

A 1-D model to specify the magnitude of inlet resistance required to inhibit flow reversal for water boiling at atmospheric pressure is presented. For the specified conditions, increasing *F* beyond a certain value (approximately 20) will not be beneficial and it only increases the pumping power. For the same conditions, the magnitudes of pressure changes estimated using the two compressibility models are almost the same. Inlet restriction can also help to suppress the flow oscillations (with the natural frequency of a spring-mass system using the upstream mass of the liquid column in the channel) that arise with trapped non-condensable gas. Future work is aimed at studying different fluids, channel dimensions, heat fluxes and nucleation site locations.

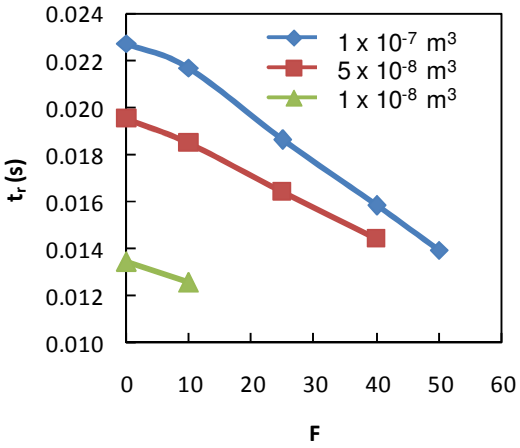

Fig. 13. Effect of inlet resistance on bubble (upstream end) return time for three different V_{ci} due to non-condensable gas.

.

Nomenclature

a_0	inlet plenum area, m^2
A	bubble projected or contact area, m^2
A_c	condensation area, m^2
A_e	evaporation area, m^2
b	partially confined bubble dimension,
C_c	linearised compressibility, m^3/Pa
D_h	hydraulic diameter, m
f	Fanning friction factor
F	inlet restriction loss coefficient
G_c	subcooled boiling compressibility parameter, Eq. (2), m^3/Ns
h	channel height, m
h_{lv}	enthalpy of evaporation, J/kg
L	length of the liquid slug
p	pressure, Pa
q	wall heat flux, W/m^2
r	ρ_v / ρ_l
Re	inlet Reynolds number

s	$A_e / V_c^{2/3}$
t	time
t_c	confinement time
t'	$t - t_c$
U	velocity, m/s
V_c	compressible volume, m^3
w	channel heated width, m
x	position of bubble
z	confined bubble length

Greek symbols

α	heat transfer coefficient, W/m^2K
β	$A_c\alpha_c / A_e\alpha_e$
γ	h / w
δ	film thickness, m
ΔT_s	superheat, K
ρ	density, kg/m^3
σ	surface tension, N/m
μ	viscosity, Ns/m^2
τ	growth time constant = $\rho_v h_{lv} h / q$

Subscripts

b	bulk liquid
c	condensation
d	downstream end
e	evaporation, exit
i	initial
l	liquid
r	return, reversal
u	upstream end
v	vapour
w	wall
sat	saturation
0	plenum, stagnation
1	channel inlet, control volume 1
2	upstream end of bubble, control volume 2,
3	downstream end of bubble

References

Agostini, B., Thome, J.R., Fabbri, M., Michel, B., Calmi, D., Kloter,U., 2008. High heat flux flow boiling in silicon multi-microchannels - Part I: Heat transfer characteristics of refrigerant R236fa, Int. J. Heat Mass Transfer 51, 5400-5414.

Brutin, D., Tadrist, L., 2004. Pressure drop and heat transfer analysis of flow boiling in a minichannel; influence of the inlet condition on two-phase flow stability, Int. J. Heat Mass Transfer 47, 2365-2377.

Gedupudi, S., Zu, Y.Q., Karayiannis, T.G., Kenning, D.B.R., Yan, Y.Y., 2011. Confined bubble growth during flow boiling in a mini/micro-channel of rectangular cross-section Part I: Experiments and 1-D modeling, Int. J. Thermal Sciences 50, 250-266.

Hartnett, J. P., Kostic, M., 1989. Heat transfer to Newtonian and non-Newtonian fluids in rectangular ducts, Advances in Heat Transfer 19, 247-356.

Kandlikar, S.G., Kuan, W.K., Willistein, D.A.,Borrelli, J., 2006. Stabilization of flow boiling in microchannelsusing pressure drop elements and fabricated nucleationsites, J. Heat Transfer 128, 389-396.

Kosar A., Kuo C.J., Peles, Y., 2006. Suppression of Boiling FlowOscillations in ParallelMicrochannels by InletRestrictors, J. Heat Transfer 128, 251-260.

Liu, Y., Fletcher, D. F., Haynes, B.S., 2013. On the importance of upstream compressibility in microchannel boiling heat transfer, Int. J. Heat and Mass Transfer 58, 503-512.

Papautsky, I., Gale, B. K., Mohanty, S., Ameel, T. A., Frazier, A.B., 1999. Effects of rectangular microchannel aspect ratio on laminar friction constant, Proc. SPIE Symposium on Micromachining and Microfabrication: MicroFluidic Devices and Systems, Santa Clara, CA, Sep. 20-21, 1999, pp. 147-158.

Wang, Y., Sefiane, K., Bennacer, R., 2011. Investigation of boiling and bubble confinement in a high aspect ratio micro-channel, Applied Thermal Engineering 31, 610-618.

White, F. M., 1994. Fluid Mechanics,3rd ed., New York, NY: McGraw Hill.

Zhang, L., Goodson, K.E., Kenny, T.W., 2004. Silicon Microchannel Heat Sinks, Theories and Phenomena, Springer Verlag, Berlin, Heidelberg, New York.

Zhang, L., Wang, E.N., Goodson, K.E., Kenny, T.W., 2005. Phase change phenomena in silicon microchannels, Int. J. Heat Mass Transfer 48, 1572–1582.